IEEE Access
Multidisciplinary ⋮ Rapid Review ⋮ Open Access Journal

Received August 18, 2020, accepted September 10, 2020, date of publication September 21, 2020, date of current version October 7, 2020.

Digital Object Identifier 10.1109/ACCESS.2020.3025349

Theoretical Investigation on Microcavity Coupler for Terahertz Quantum-Well Infrared Photodetectors

XUGUANG GUO[1], YUXIANG REN[1], GUIXUE ZHANG[1], ANQI YU[1,3], XIAOSHUANG CHEN[2], AND YIMING ZHU[1,3]

[1]Shanghai Key Laboratory of Modern Optical System, Terahertz Spectrum and Imaging Technology Cooperative Innovation Center, Terahertz Technology Innovation Research Institute, University of Shanghai for Science and Technology, Shanghai 200093, China
[2]National Laboratory for Infrared Physics, Shanghai Institute of Technical Physics, Chinese Academy of Sciences, Shanghai 200083, China
[3]Shanghai Institute of Intelligent Science and Technology, Tongji University, Shanghai 200092, China

Corresponding authors: Xuguang Guo (xgguo_sh@qq.com), Xiaoshuang Chen (xschen@mail.sitp.ac.cn), and Yiming Zhu (ymzhu@usst.edu.cn)

This work was supported in part by the National Natural Science Foundation of China under Grant 61731020 and Grant 61722111, in part by the National Key Research and Development Program of China under Grant 2017YFA0701005, in part by the 111 Project under Grant D18014, in part by the International Joint Laboratory Program, Science and Technology Commission, Shanghai Municipality, under Grant 17590750300, and in part by the Young Yangtse River Scholar under Grant Q2016212.

ABSTRACT Resonant behaviors and absorption enhancement of metallic grating-dielectric-metal (GDM) microcavity are theoretically investigated. The GDM structure is treated as periodic unit cells of two serially-connected metal-dielectric-metal (MDM) and air-dielectric-metal (ADM) waveguide resonators. The resonant modes can be divided into three types: the LC mode, the TEM modes supported by the MDM waveguide resonator, and the TEM-TM hybrid modes supported by the whole GDM structure. The resonant frequencies of LC and TEM modes are independent on a small incident oblique angle. However, for the TEM-TM hybrid modes, each mode splits into two branches with non-zero incident angles. Based on the temporal coupled-mode theory, the intersubband absorption efficiency of multi quantum wells inserted into the GDM microcavity is calculated and discussed qualitatively. We point out that the condition of critical coupling is not the optimal condition for intersubband absorption efficiency when the metallic loss cannot be neglected. An optimization procedure is given for the design of high performance GDM-microcavity-coupled terahertz quantum-well infrared photodetectors.

INDEX TERMS Terahertz photodetectors, microcavity, critical coupling, grating, waveguide, quantum well.

I. INTRODUCTION

Since the first demonstration of quantum-well infrared photodetector (QWIP) by Levine *et al.* [1]a, great progresses have been achieved both in the device physics and the fabrication of large-scale focal-plane-array imagers working in mid- and far-infrared regions (3-5 μm and 8-14 μm) [2]. In terahertz spectral region, because of the very small photon energy, there are no terahertz photodetectors based on interband transitions of natural bulk materials. As important photon-type terahertz detectors, terahertz QWIPs have been realized in 2004 [3]. Advantages of single-element terahertz QWIPs, such as high sensitivity and fast response speed, have been demonstrated [4]–[6]. The prototype terahertz pixel-less imager based on QWIP-LED (light emission diode) frequency up-converter has been realized [7]. Because of the high-quality GaAs/AlGaAs multi quantum wells (MQWs) and mature fabrication techniques [2], it is expected that large-scale terahertz QWIP focal plane arrays will be fabricated under the boost of terahertz imaging applications in the near future.

For n-type QWIPs, the photon detection is based on the intersubband transition of confined electrons in the MQWs. The quantum selection rule of intersubband transition determines that the normally incident light (the propagation direction perpendicular to the QW plane) cannot excite such a transition. Brewster-angle incidence [2], fabrication of oblique incident facet [2], and grating [8]–[10] are utilized to obtain the electric field component perpendicular to the QW plane, which can induce intersubband transitions. In terahertz QWIPs, because of the small energy difference between the ground subband and the first

The associate editor coordinating the review of this manuscript and approving it for publication was Bora Onat.

excite subband, the electron doping concentration in QWs is severely limited, which leads to the ultra-low intersubband absorption efficiency (IAE, <5%) [3]. Low IAE not only weakens the responsivity, but also introduces additional generation-recombination noise [2]. Different type microcavities composed of upper structured metal film (one-dimensional (1D) grating or two-dimensional (2D) periodic structure), MQW layer, and bottom metal mirror, have been proposed and fabricated [4], [12]–[14]. In such a microcavity-coupled QWIP, at some resonant frequencies, the electromagnetic energy can be effectively funneled into the microcavity and be localized in the subwavelength MQW region [15]. Moreover, the direction of incident electric field can be changed by the upper structured metal film along the growth direction of MQW. The above properties of microcavity are more important for terahertz QWIPs because of low IAE and deep subwavelength thickness of MQW absorption layer.

There are many investigations on the optical properties of the above microcavity-MQW structures due to the interaction of resonant modes and intersubband transitions. Todorov *et al* developed and implemented a simulation tool for grating-dielectric-metal (GDM) structures with high computational efficiency based on modal method (MM) [16], [17], and combined with a semi-analytical theory, the properties of resonant modes, field enhancement, and IAE were systemically studied [17]. Further, the strong coupling phenomena between the resonant modes supported by GDM microcavity and intersubband transitions were thoroughly explored both in theoretical and experimental aspects [18]–[20]. The effects of critical coupling on absorption efficiency were investigated and optimal conditions for improving absorption were derived [21]–[24]. Palaferri *et al* designed and fabricated a microcavity-coupled QWIP with a peak response frequency of 9 μm and superior performance parameters (high sensitivity, fast response time, and operation at room temperature) [25]. Palaferri *et al.* [4], Chen *et al.* [26], and Zheng *et al.* [27], [28] realized high-performance microcavity-coupled terahertz QWIPs. Other interesting phenomena related to the coupled microcavity-QW systems, such as giant nonlinear coefficient at terahertz frequencies [29] and bound states in continuum [30] have been studied.

In the previous investigations on GDM structures, only the transverse electromagnetic (TEM) modes supported by the metal-dielectric-metal (MDM) section of GDM structure are considered, and because of the discontinuity of refractive indexes near the edges of metal strip, a MDM waveguide resonator is formed [17]. For each mode, an effective refractive index is introduced. However, when the dimension of metallic periodic structure is not very much smaller than the wavelength, the effective refractive index is not always a useful and predictive concept [31], [32]. Meanwhile, for intersubband absorption efficiency (IAE), the difference between the critical-coupling and the optimal conditions for IAE and the role of metal loss are not well addressed.

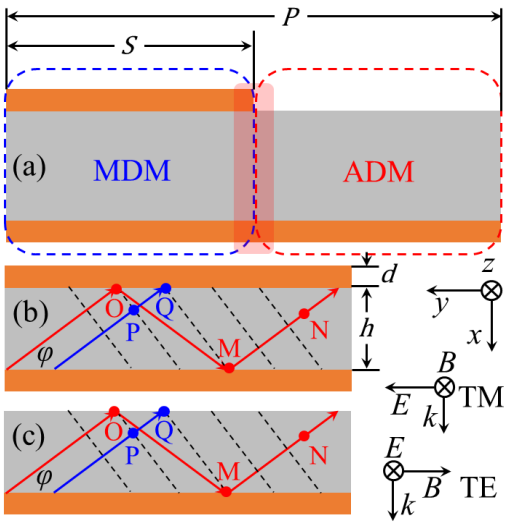

FIGURE 1. Schematic of the metal-grating-MQW-metal structure (a), light rays and the constant phase fronts (black dash lines) for the MDM waveguide (b) and the ADM waveguide (c). *P* is the periodicity of grating and *S* is the width of metal strip.

In this paper, we focus on two problems of GDM-microcavity-coupled terahertz QWIPs, the origins of resonant modes and the optimal condition for improving IAE. Based on the light-ray method [33], the dispersion relations of resonant waveguide modes of the MDM waveguide and the air-dielectric-metal (ADM) waveguide are calculated. The GDM structure is treated as a serially-connected MDM and ADM waveguides [34]. Due to the mismatch of mode dispersions of the MDM and ADM structures, two serially-connected MDM-waveguide resonator and ADM-waveguide resonator are formed. Equivalent circuit method (ECM) [35], [36], the COMSOL package (version 3.5a) [37], and the MM [16] are used to explore the optical properties of the GDM structure. A LC mode, TEM modes, hybrid TEM-transverse magnetic (TM) modes, and grating diffractive modes can be excited by incident TM plane waves. The temporal coupled-mode theory (TCMT) [38] is used to discuss the optimization of IAE. The metallic loss is always playing a negative role in the improvement of IAE. A design and optimization procedure is given for designing high-performance GDM-microcavity-coupled terahertz QWIPs.

II. RESONANT-MODE FREQUENCIES OF THE MICROCAVITY

Fig. 1(a) shows the microcavity structure considered in this paper. In general, the microcavity is composed of a metal grating, a subwavelength MQW structure grown along the x direction, and a bottom metal mirror. In terahertz frequency range, due to its excellent material quality, the GaAs/AlGaAs material system is used to realize the MQW structure. Due to the excitation of optical phonon and the intersubband transitions, the refractive index of MQW is a complex function of frequency. In this work, we focus on the origins of resonant modes of the microcavity, therefore, we do not consider the complicated dispersion behavior of the MQW, which is very

important for the design and optimization of a device having a given resonant frequency. Because the Al mole fraction in AlGaAs barrier is very low (<5%) [2] in terahertz QWIPs, for simplicity, a uniform 3-μm thick insulator layer having a constant refractive index of 3.5-0.01i with i the imaginary unit (the approximate value of GaAs refractive index at about 4.0 THz) is used to substitute the MQW layer. Such an approximation is very helpful for exploring the origins of the resonant modes and has no essential influence on our main conclusions. Following Refs. [17], [34], the microcavity is treated as a periodic structure in y direction; each unit cell is composed of two serially-connected MDM and ADM waveguides. Due to the mismatch of mode dispersion relations supported by the MDM and ADM waveguides, the lateral propagation modes in the MDM and ADM waveguides will suffer strong reflection on the interface (marked by the semi-transparent red bar in Figure 1(a)) between the MDM and ADM waveguides. Therefore, two serially-connected MDM and ADM resonators are formed. Based on such a model, many resonant properties of the GDM microcavity are well understood [17].

For TM incident waves (the electric field along y direction, perpendicular to the grating metal strips), due to the dipolar interaction, the metal strip can be effectively excited and behaves as a secondary wave source. Through such a mechanism, the free-space TM waves can be effectively coupled into the MDM and ADM resonators at the resonant frequencies. It is expected that the resonant behaviors are determined by the structural parameters of thickness h of the dielectric layer (dispersion relations of MDM and ADM resonant waveguide modes), the width S of metal strip (the lateral dimension of MDM resonator), and the periodicity P (the lateral dimension of ADM resonator and the diffraction modes of grating). Moreover, the interaction between the MDM and ADM resonators cannot be ignored.

As shown in Fig. 1, for the 1D-GDM structure, only the modes with electric fields perpendicular to the z axis (TM modes) can be launched by the grating. Therefore, the transverse-electric modes (electric fields parallel to the z axis, TE) are not considered. For the MDM waveguide, the TEM mode with zero cutoff frequency is the fundamental mode. However, the TEM mode cannot be supported by the ADM waveguide [39]. The TM modes with the electric field perpendicular to the propagation direction and in xy plane can also be supported by the MDM and ADM waveguide. As shown in Figs. 1(b) and 1(c), the light-ray method [33] is adopted to solve the eigenmode problem. As shown in Figs. 1(b) and 1(c), PQ and MN are two parallel rays. For guided modes, OP and QM must be two equiphase surfaces. Therefore, the following condition must be satisfied for the TM modes,

$$(k_0 n_1 L_2 + \Phi_L + \Phi_U) - k_0 n_1 L_1 = 2m\pi, (m = 1, 2, 3 \ldots) \tag{1}$$

where $k_0 = 2\pi/\lambda$ is the wavevector in vacuum with λ the wavelength, n_1 is the refractive index of dielectric in the waveguide, Φ_L (Φ_U) is the additional reflection phase at the bottom (upper) interface of waveguide, L_1 (L_2) is the optical path of the blue (red) ray shown in Figs. 1(b) and 1(c), and m is an integer. The optical paths L_1 and L_2 are

$$L_1 = \overline{PQ} = h\left(\frac{1}{\sin\varphi} - 2\sin\varphi\right), \quad L_2 = \overline{OM} = \frac{h}{\sin\varphi} \tag{2}$$

where h is the thickness of waveguide. For the MDM waveguide, $\Phi_L = \Phi_U = \pi$, the dispersion relations of TM modes are expressed as

$$k_0 n_1 h \sin\varphi = m\pi, \quad (m = 1, 2, 3 \ldots) \tag{3}$$

For the ADM structure, the additional reflection phases are [33]

$$\Phi_L = \pi, \quad \Phi_U = -2\tan^{-1}\frac{\sqrt{n_1^2\cos^2\varphi - n_0^2}}{n_1\sin\varphi} \tag{4}$$

where $n_0 = 1$ is the vacuum refractive index. By substituting Eq. (4) into Eq. (1), the dispersion relations of TM modes for the ADM waveguide are

$$\tan\left(k_0 n_1 \sin\varphi - \frac{2m-1}{2}\pi\right) = \frac{\sqrt{n_1^2\cos^2\varphi - n_0^2}}{n_1\sin\varphi}, \quad (m = 1, 2, 3 \ldots) \tag{5}$$

The RF module included in COMSOL package is used to compute the reflection spectra of two GDM microcavities with a very large duty cycle (29/30, L-GDM) and a very small duty cycle (1/30, S-GDM). For perfect MDM and ADM waveguides, the guided modes cannot be excited by the plane waves propagating perpendicular to the waveguide surface. Therefore, the L-GDM (29/30) and the S-GDM (1/30) structures are used to mimic the perfect MDM and ADM waveguides, respectively. A plane wave propagating along the x direction is set to drive the structure. Floquet periodic boundary conditions are used in y direction, and on top of the simulation domain, a perfect match layer is added to absorb the reflection wave propagating along the x direction. Au is used to construct the metal strip of grating and the bottom mirror. The permittivity of Au is described by the Drude model with the plasma angular frequency of 1.11×10^{16} Hz and the scattering rate of 8.33×10^{13} Hz [40]. The meshing parameters and the air thickness above the grating are verified to assure the accuracy of numerical results. Fig. 2(a) presents the reflection spectrum of L-GDM structure (MDM waveguide). There are a high-reflectance background and a series of reflection sharp dips due to the excitation of resonant modes. For the S-GDM structure (ADM waveguide), there is a broad reflection dip due to Fabry-Perot resonance and a series of shallow dips superposing over the broad dip. To further identify the resonant modes supported by the MDM and ADM waveguides, Eqs. (1) and (5) are numerically solved to obtain the dispersion relations of waveguide resonant modes and the results are shown in Fig. 2(c). There are a fundamental TEM mode and a TM_1 mode supported by the MDM waveguide and TM_1 and TM_2 modes supported by the ADM waveguide in the frequency range of 0-16 THz.

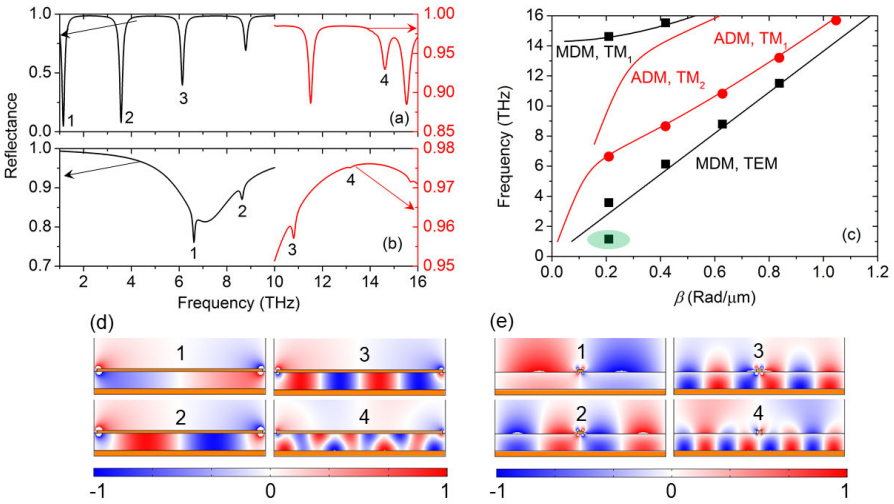

FIGURE 2. Reflection spectra of the GDM structure with a large duty cycle (29/30, L-GDM, mimicking the MDM structure) (a) and with a small duty cycle (1/30, S-GDM, mimicking the ADM structure) (b), (c) the dispersion relations of the MDM and ADM waveguides for the first two modes (lines) and the computational data by using COMSOL package (scatters), and electric field (x-component) distributions of the marked reflection dips (d) shown in (a) and (e) shown in (b).

The normalized mode electric-field (E_x) distributions at the resonant frequencies corresponding to the marked reflection dips shown in Fig. 2(a) are presented in Figs. 2(e) and 2(f), from which the finite propagation constant $\beta = 2\pi n/P$ with n an integer can be determined. Once the value of β is determined, the numerical dispersion relations of resonant mode computed with the COMSOL package can be obtained, which are depicted as scatters in Fig. 2(b). Except the first dip for the L-GDM (MDM) structure, the numerical data are in good agreement with the theoretical dispersion relations calculated by solving Eqs. (1) and (5).

The first reflection dip marked by a green ellipse in Fig. 2(c) does not originate from the TEM or TM modes supported by the MDM structure because the data point is not on any dispersion-relation curves. As shown in Fig. 2(d), the mode electric field distributions of the first and second reflection dips are very different, which further indicates that the first reflection dip is not induced by TEM-mode-induced resonance. Popov *et al.* [41] have shown that shallow 1D metallic gratings can show a metamaterial behavior. This reflection dip is attributed to the LC resonance supported by the GDM microcavity structure. At low frequency, the ECM [35] is adopted to describe the LC-resonant-induced reflection dip. The equivalent circuit of the microcavity is shown in Fig. 3(a). The lumped impendences in Fig. 3(a) for normally incident TM waves are [34]

$$Z_1 = i\frac{\omega\mu_0}{n_1 k_0}\tan\left(n_1 k_0 h\right), \quad Z_0 = \sqrt{\frac{\mu_0}{\varepsilon_0}} \tag{6}$$

$$Z_g = \frac{i\pi Z_0}{2k_0 n_{eff}^2 \ln\left(\sin\frac{P-S}{2P}\right)}, \quad n_{eff} = \sqrt{\frac{n_1^2+1}{2}} \tag{7}$$

$$Z_{\text{in}} = \frac{Z_g Z_1}{Z_g + Z_1} \tag{8}$$

where Z_1 is the impedance of the dielectric layer and the bottom metallic mirror, ω is the angular frequency of

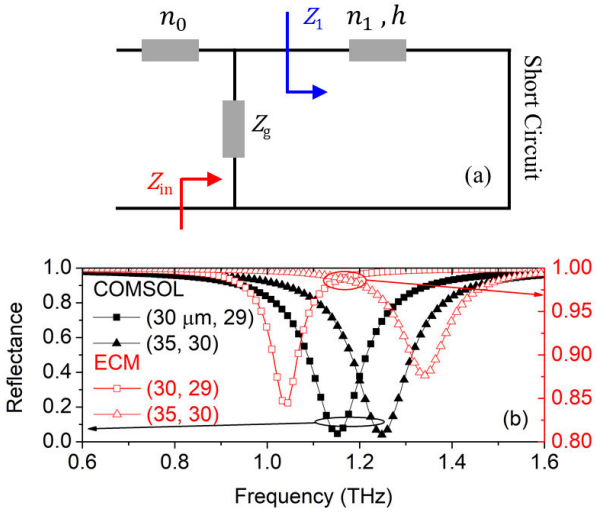

FIGURE 3. (a) Equivalent circuit of the microcavity and (b) the reflection spectra near the first reflection dip calculated by using ECM and COMSOL for ($P = 30$ μm, $S = 29$ μm) and ($P = 35$ μm, $S = 30$ μm), respectively.

incident wave, μ_0 is the vacuum permeability, Z_g is the lumped impedance of the metal grating with large duty cycle ($P \subset S \ll P$), $Z_0 = 377\Omega$ is the vacuum impedance, ε_0 is the vacuum permittivity, n_{eff} is the effective refractive index, and Z_{in} is the input impedance of the microcavity. When Z_{in} is obtained, the reflection spectrum is calculated with the expression

$$R(\omega) = r(\omega)\, r(\omega)^*, \quad r(\omega) = \frac{Z_{in}(\omega) - Z_0}{Z_{in}(\omega) + Z_0} \tag{9}$$

where $R(\omega)$ and $r(\omega)$ are the power and amplitude reflection spectra, respectively.

Fig. 3(b) shows the reflection spectra of the GDM microcavity with different duty cycle (29/30 and 30/35) at low frequency range calculated by using the ECM and the COMSOL package. Because the near-field effects (evanescent high-order modes) are not considered in the ECM,

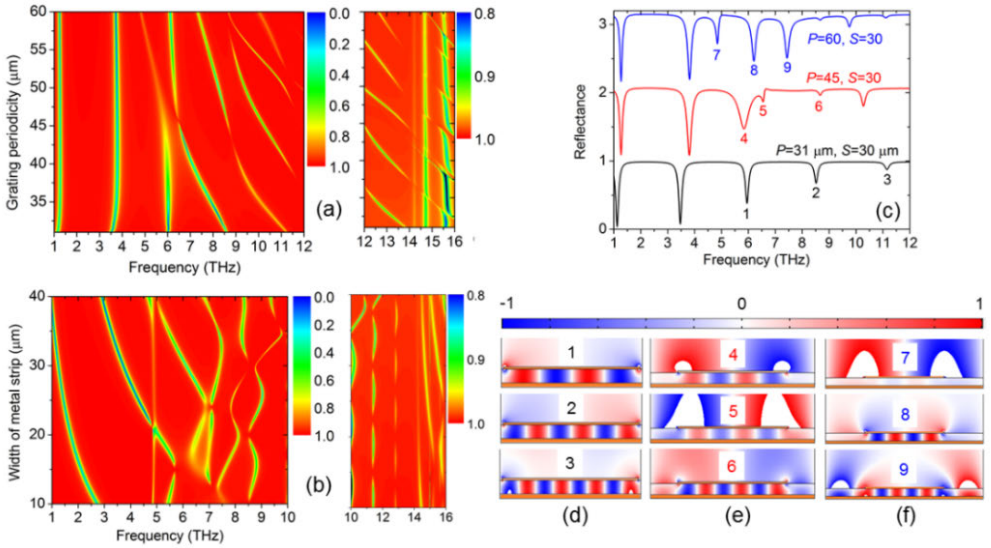

FIGURE 4. Numerical false-color contours of reflection spectra of the microcavities with a fixed metallic strip width of 30 μm and a sweeping of grating periodicity from 31 μm to 60 μm (a) and a fixed grating periodicity of 60 μm and a sweeping of metallic strip width from 10 μm to 40 μm (b) calculated by using the MM, (c) reflection spectra of microcavities with different parameter configurations, distributions of mode electric fields at the marked reflection dips for different parameter configurations of $P = 31$ μm and $S = 30$ μm (d), $P = 45$ μm and $S = 30$ μm (e), and $P = 60$ μm and $S = 30$ μm (f).

there are notable discrepancies of resonant frequencies and power reflection amplitudes with different grating periodicities and duty cycles (29/30 and 30/35) between the results calculated by using the ECM and the COMSOL package. Especially for the deep subwavelength microcavity ($h \ll \lambda_0$), near-field effects will play key roles on the LC resonance. Therefore, in the qualitative level, the numerical results obtained from the ECM indicate that the first reflection dip shown in Fig. 2(a) originates from the LC resonant mode.

For the L-GDM and S-GDM structures, the resonant modes are solely supported by the MDM and ADM waveguide resonators, respectively. However, in realistic situations, in order to obtain a high excitation efficiency, an intermediate duty cycle is superior. In such a GDM structure with an intermediate duty cycle, the resonant behaviors are more complicated. In Fig. 4(a), the reflection spectra (false-color contours) of the GDM structure with a fixed metal strip width and a sweeping of grating periodicity from 31 μm to 60 μm is computed by using the fast MM with an impedance match approximation [16]. For the grating periodicity and the frequency considered in this work, the impedance match approximation should give correct results [16]. The homemade code based on MM is thoroughly tested. Normally incident TM plane waves is adopted to excite the structure. The reflection spectra shown in Fig. 4(a) can be divided into three regions, 1-6 THz, 6-14 THz, and 14-16 THz. In the first and the third regions, the frequencies of the reflection dips do not shift with the increase of grating periodicity, which indicates that the mode electric fields are localized underneath the metal strip. Fig. 2(c) shows that the reflection dips in the first and third regions correspond to the LC, TEM, and TM_1 modes supported by the MDM resonator, respectively. On the contrary, in the second region, all the reflection dips shift to lower frequencies with increasing the grating periodicity. An anti-crossing behavior between the third and fourth dips occurs with the parameter P in the range of 42-47 μm. In Fig. 4(b), the reflection spectra (false-color contours) of the GDM microcavity with a fixed grating periodicity of $P = 60$ μm and a sweeping of metal strip width $S = 10$-40 μm are presented. In the first and third regions, the frequencies of the reflection dips monotonously decrease with the increase of metal strip width. In the second region, the reflection spectra show very complex behaviors. The above results indicate that the resonant modes with their frequencies located in the second region are not solely supported by the MDM or ADM resonators. Fig. 4(c) shows three reflection spectra with a fixed metal strip width of 30 μm and grating periodicities of $P = 31$, 45, and 60 μm, respectively. Three groups of reflection dips are marked, (1, 4, and 8), (2, 5, and 7), and (3, 6, and 9), and their electric field (E_x) distributions are depicted in Figs. 4(d), 4(e), and 4(f), respectively. The electric field distributions show that the first group of dips (1, 4, and 8) correspond to the second-order TEM modes. In the second and third groups, dips 2, and 3 correspond to the third and fourth TEM modes, respectively; dips 5, 6, and 9 correspond to the hybrid modes supported by the GDM microcavity. Dip 7 is different from the other dips, which corresponds to the grating-induced first diffraction mode.

Incident-angle-dependent behaviors of resonant mode do not only play key roles on the photoresponse of microcavity-coupled terahertz QWIPs because the incident terahertz radiation is a focused beam, but also provide additional information of the resonant modes. Fig. 5 shows the reflection spectra of the GDM microcavity with $P = 60$ μm and $S = 30$ μm at different incident angles. The frequencies

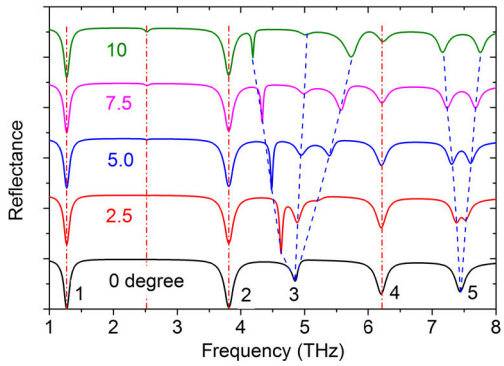

FIGURE 5. Reflection spectra with different incident angles for the microcavity with $P = 60\ \mu$m and $S = 30\ \mu$m.

of modes 1, 2 and 3 are incident angle independent. For the LC resonant mode 1, because the thickness of the microcavity is in deep subwavelength scale, for a small incident angle, the incident-angle-dependent propagation effect can be neglected. The dips 2 and 4 correspond to the first and second TEM modes, respectively. There are no x components of the wavevectors for the TEM modes, and the conservation law of momentum must lead to the same propagation constant for the forward and backward propagation modes, which restricts the incident-angle-induced frequency splitting of the two modes. The reflection dip 3 originates from the first grating diffractive mode. For TM incident waves, the grating introduces y-components of wavevector $k_y = 2\pi n/p + k_0 \sin\theta$ with $n = \pm 1, \pm 2, \ldots$ and θ the incident angle. Therefore, for non-zero incident angles, the forward and backward propagation modes have different propagation constants, which lifts the degeneracy existing in the case of normal incidence. As shown in Fig. 4(f) (dip 9), the dip 5 in Fig. 5 is a TEM-TM hybrid mode, thus a small effective x component of wavevector exists, which results in the splitting of dip 5. There are two extra reflection dips at non-zero incident angles, which originate from the even dark modes. The incident-angle-dependent photoresponse of GDM-microcavity-coupled THz QWIPs has been found experimentally [27]. For a larger oblique angle, the angle-dependent behaviors obey the same rule. In general, for the microcavity terahertz QWIPs, only the normally incident case and the small oblique angle case are considered. Therefore, the numerical results for larger oblique angles (>10 degrees) are not included in Fig. 5.

III. CRITICAL COUPLING AND OPTIMIZATION OF INTERSUBBAND ABSORPTION EFFICIENCY

IAE is a key figure of merit for terahertz QWIPs (enhancing responsivity and suppressing generation-recombination noise) [2]. There are several investigations on the IAE of microcavity-coupled terahertz QWIPs based on numerical calculations and quasi-analytical models [17], [23], [24]. Meanwhile, perfect absorbers and critical-coupling phenomena have become a hot research subject for several years [20]–[22]. We propose a qualitative model based on the TCMT [38] to discuss the IAE of microcavity-coupled terahertz QWIPs. The TCMT is a powerful framework to analysis various mode coupling phenomena. However, the TCMT is not a first-principle method, and the technical details are encapsulated into the coupling and loss parameters. The accuracy of TCMT is dependent on the coupling and loss parameters. Therefore, the TCMT is usually used to qualitatively analysis the mode coupling behaviors and to fit the experimental data and the rigorous numerical results. A microcavity-coupled terahertz QWIP can be considered as a one-port resonator including one resonant mode. The field amplitude a of the resonant mode is [38]

$$\frac{da}{dt} = i\omega_0 a - \left(\frac{1}{\tau_0} + \frac{1}{\tau_e}\right) a + \sqrt{\frac{2}{\tau_e}} s \tag{10}$$

where ω_0 is the frequency of resonant mode, τ_0 is the decay time due to loss, τ_e is the radiation coupling time, and s is the amplitude of input wave. The decay time τ_0 can be divided into two parts $1/\tau_0 = 1/\tau_{QW} + 1/\tau_m$, where τ_{QW} and τ_m are the decay times due to intersubband absorption and metal loss, respectively. For simplicity, the free electron absorption in the contact layers and other dielectric losses are lumped into the metal loss decay time τ_m. The solution of Eq. (10) is [38]

$$a(t) = \frac{\sqrt{2/\tau_e} s}{i(\omega - \omega_0) + 1/\tau} \left[e^{i\omega t} - e^{\left(i\omega_0 - 1/\tau\right) t} \right] \tag{11}$$

where ω is the frequency of driven field and $1/\tau = 1/\tau_0 + 1/\tau_e$ is the total decay rate. In steady state and at the resonant frequency ω_0, the energy W stored in the resonator is

$$W = a(t)\, a(t)^* = \frac{2\tau^2}{\tau_e} s s^* = \frac{2\tau^2}{\tau_e} P_{in} \tag{12}$$

where P_{in} is the input power. The intersubband absorption efficiency can be expressed as

$$\eta = \frac{2}{\tau_{QW}} \times W \times \frac{1}{P_{in}} = \frac{4\tau^2}{\tau_e \tau_{QW}} \tag{13}$$

After some algebra, η can be transformed to

$$\eta = \frac{4C}{(1+C)^2} - \frac{4C^2}{(1+C)^2 x} \quad (x > C) \tag{14}$$

where $C = \tau_0/\tau_e$ and $x = \tau_m/\tau_e$ are the reduced total and metal decay times, respectively. The values of $C > 1$, $C < 1$ and $C = 1$ correspond to the over-coupled, under-coupled, and critically-coupled cases, respectively. Eq. (14) indicates that at a fixed value of reduced total decay time C (corresponding to a fixed reflectance coefficient), the value of IAE η monotonically decreases with the decrease of reduced metallic decay time x. For given parameters C and x, the reduced decay time of intersubband absorption $y = \tau_{QW}/\tau_e$ and the reflectance coefficient R can be determined by

$$y = \frac{Cx}{x - C} \tag{15}$$

and

$$R = \left(\frac{C-1}{C+1}\right)^2 \tag{16}$$

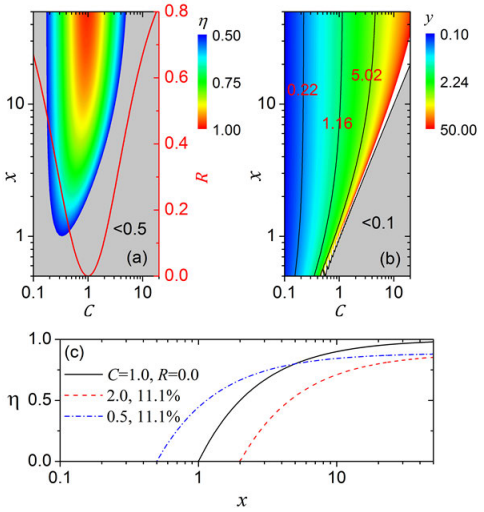

FIGURE 6. IAE as a function of reduced total and metal loss decay times C and x. (a) False-color contour of intersubband absorption efficiency for $C = 0.1$-20 and $x = 0.1$-50 and the reflection coefficient as a function of C, (b) False-color contour of the reduced decay time y due to MQW intersubband absorption (in logarithmic scale), and (c) IAEs as functions of reduced metal loss decay time for $C = 1.0$ (critically coupled), 2.0 (over coupled), and 0.5 (under coupled).

For critical coupling, zero reflectance is reached, which is important for perfect absorbers. However, for terahertz QWIPs, the intersubband absorption efficiency is the most important parameter. The intersubband absorption efficiency η with respect to parameters C and x is calculated and depicted in Fig. 6(a) for $\eta > 50\%$. There is a considerable region in which the value of IAE is larger than 50%. For terahertz QWIPs, in order to suppress the dark current, the doping concentration in the MQW is severely limited, which results in the very low IAE (<5%) in traditional 45-degree-facet-coupled terahertz QWIPs [2]. Fig. 6(b) shows the reduced decay time y ($0.5 < y < 50$) due to intersubband absorption with respect to parameters C and x. To achieve a large IAE of $\eta > 50\%$, parameters x and y should be in the ranges of $x > 1$ and $0.2 < y < 5.0$, respectively. Therefore, for a fixed value of C, the IAE will be always improved by reducing the metallic losses introduced by the metallic grating structure, the bottom metal mirror, and the top and bottom Ohmic contacts. For terahertz QWIPs, the intersubband-absorption-induced decay time cannot be very short due to low electron doping concentration in the MQW region. The TCMT results indicate that the microcavity-coupled terahertz QWIPs have a good property that in a broad range of y, the IAE is larger than 50%. As shown in Fig. 6(b), for the same reflection coefficient and the metal loss decay time, the under-coupled case is more beneficial to enhance IAE and has a better tolerance to the metal loss. The IAE is not explicitly dependent on the radiation coupling time τ_e. However, τ_e is a key parameter to determine the performance of device. A smaller value of coupling (radiating) time τ_e will show a good tolerance to poor-quality metals and enhance the response spectral bandwidth. On the other hand, with the decrease of τ_e, the intersubband-absorption-related decay time τ_{QW} must be proportionally decreased to maintain high IAE, which can be realized by increasing the electron doping concentration in the MQW region. However, the high doping concentration will result in the fast increase of dark current and then degrades the device performance.

The radiation coupling time of a resonant mode is independent on the loss properties of materials composed of the microcavity in the low-loss approximation. Instead, the structural parameters, the width of metal strip, the periodicity of grating, the thickness of dielectric layer sandwiched between the grating and the bottom mirror, and the height of metallic strip, determine the radiation coupling time. The other two decay times, τ_m and τ_{QW}, are related to not only the metal loss and intersubband absorption, but also the mode electric-field distribution. Despite there are many theoretical efforts to calculate the three parameters [17], [20]–[24], it is still a hard task to find the optimal coupling conditions theoretically for microcavity-coupled terahertz QWIPs. Following the above discussions based on TCMT, a design and optimization procedure can be given. Firstly, traditional 45-degree-facet-coupled terahertz QWIPs can be designed and fabricated. The dependences of dark current and the decay time τ_{QW} due to intersubband absorption on the doping concentration are determined. Moreover, the peak response frequency and then the averaged refractive index of MQW are obtained. To ensure the Ohmic contacts, minimal values of doping concentration in the upper and bottom contact layers and the thicknesses of the contacts should be reached, which is beneficial for realizing high IAE. Secondly, from Fig. 6, the structural parameters of the microcavity are optimized to obtain the appropriate value of τ_e. Lastly, the metal loss should be evaluated and further minimized.

IV. CONCLUSION

In summary, resonant behaviors and IAE enhancement of GDM microcavity are theoretically investigated. The GDM structure is treated as a periodic serially-connected MDM waveguide and ADM waveguide. Because of the mismatch of mode dispersions between the MDM and ADM waveguides, the MDM and ADM waveguide resonators are formed. The mode dispersion relations of MDM and ADM waveguides are calculated based on the light-ray method. The reflection spectra of the GDM microcavity with very small and large grating duty cycles are computed by using the RF module integrated in the COMSOL package, respectively, and the resonant mode dispersion relations are derived, which are in good agreement with the theoretical dispersion relations of MDM and ADM waveguides calculated within the light-ray method. The ECM, the MM with an impedance match approximation, and the COMSOL package are used to identify the origins of resonant modes supported by the GDM structures. They are the LC mode, the first-order diffractive mode, TEM modes supported by the MDM waveguide resonator, and the TEM-TM hybrid modes supported by the whole GDM structure. The resonant frequencies of LC and TEM modes are independent on incident oblique angle when

the value of incident angle is not very large, which is beneficial for improving the photoresponse of GDM-microcavity-coupled terahertz QWIPs. However, for the grating diffractive mode and the TEM-TM hybrid modes, each mode will split into two branches with non-zero incident angle. Based on TCMT, the IAE of MQWs inserted into the GDM microcavity is calculated and discussed qualitatively. We point out that the condition of critical coupling is not the optimal one for the enhancement of IAE when the metal loss cannot be neglected. An optimization procedure is given for the design of high performance GDM-microcavity-coupled terahertz QWIPs.

REFERENCES

[1] B. F. Levine, K. K. Choi, C. G. Bethea, J. Walker, and R. J. Malik, "New 10 μm infrared detector using intersubband absorption in resonant tunneling GaAlAs superlattices," *Appl. Phys. Lett.*, vol. 50, no. 16, pp. 1092–1094, Apr. 1987.

[2] H. Schneider and H. C. Liu, *Quantum Well Infrared Photodetectors: Physics and Applications*. Berlin, Germany: Springer, 2007.

[3] H. C. Liu, C. Y. Song, A. J. SpringThorpe, and J. C. Cao, "Terahertz quantum-well photodetector," *Appl. Phys. Lett.*, vol. 84, no. 20, pp. 4068–4070, Mar. 2004.

[4] D. Palaferri, Y. Todorov, Y. N. Chen, J. Madeo, A. Vasanelli, L. H. Li, A. G. Davies, E. H. Linfield, and C. Sirtori, "Patch antenna terahertz photodetectors," *Appl. Phys. Lett.*, vol. 106, no. 16, Apr. 2015, Art. no. 161102.

[5] X. G. Guo, J. C. Cao, R. Zhang, Z. Y. Tan, and H. C. Liu, "Recent progress in terahertz quantum-well photodetectors," *IEEE J. Sel. Topics Quantum Electron.*, vol. 19, no. 1, Jan. 2013, Art. no. 8500508.

[6] H. Li, W.-J. Wan, Z.-Y. Tan, Z.-L. Fu, H.-X. Wang, T. Zhou, Z.-P. Li, C. Wang, X.-G. Guo, and J.-C. Cao, "6.2-GHz modulated terahertz light detection using fast terahertz quantum well photodetectors," *Sci. Rep.*, vol. 7, no. 1, p. 3452, Jun. 2017.

[7] Z. L. Fu, L. L. Gu, X. G. Guo, Z. Y. Tan, W. J. Wan, T. Zhou, D. X. Shao, R. Zhang, and J. C. Cao, "Frequency up-conversion photon-type terahertz imager," *Sci. Rep.*, vol. 6, no. 1, p. 25383, May 2016.

[8] K. W. Goossen and S. A. Lyon, "Grating enhanced quantum well detector," *Appl. Phys. Lett.*, vol. 47, no. 12, pp. 1257–1259, Dec. 1985.

[9] J. Y. Andersson and L. Lundqvist, "Near-unity quantum efficiency of AlGaAs/GaAs quantum well infrared detectors using a waveguide with a doubly periodic grating coupler," *Appl. Phys. Lett.*, vol. 59, no. 7, pp. 857–859, Aug. 1991.

[10] Y. Andersson and L. Lundqvist, "Grating-coupled quantum-well infrared detectors: Theory and performance," *J. Appl. Phys.*, vol. 71, no. 7, pp. 3600–3610, Jan. 1992.

[11] L. Lundqvist, J. Y. Andersson, Z. F. Paska, J. Borglind, and D. Haga, "Efficiency of grating coupled AlGaAs/GaAs quantum well infrared detectors," *Appl. Phys. Lett.*, vol. 63, no. 24, pp. 3361–3363, Dec. 1993.

[12] W. A. Beck and M. S. Mirotznik, "Microstrip antenna coupling for quantum-well infrared photodetectors," *Infr. Phys. Technol.*, vol. 42, nos. 3–5, pp. 189–198, Jun. 2001.

[13] X. Guo, R. Zhang, J. Cao, and H. Liu, "Numerical study on metal cavity couplers for terahertz quantum-well photodetectors," *IEEE J. Quantum Electron.*, vol. 48, no. 5, pp. 728–733, May 2012.

[14] Q. Li, Z. Li, N. Li, X. Chen, P. Chen, X. Shen, and W. Lu, "High-polarization-discriminating infrared detection using a single quantum well sandwiched in plasmonic micro-cavity," *Sci. Rep.*, vol. 4, no. 1, p. 6332, Sep. 2014.

[15] G. Quaranta, G. Basset, O. J. F. Martin, and B. Gallinet, "Recent advances in resonant waveguide gratings," *Laser Photon. Rev.*, vol. 12, no. 9, Jul. 2018, Art. no. 1800017.

[16] Y. Todorov and C. Minot, "Modal method for conical diffraction on a rectangular slit metallic grating in a multilayer structure," *J. Opt. Soc. Amer. A, Opt. Image Sci.*, vol. 24, no. 10, pp. 3100–3114, Oct. 2007.

[17] Y. Todorov, L. Tosetto, J. Teissier, A. M. Andrews, P. Klang, R. Colombelli, I. Sagnes, G. Strasser, and C. Sirtori, "Optical properties of metal-dielectric-metal microcavities in the THz frequency range," *Opt. Express*, vol. 18, no. 13, pp. 13886–13907, Jun. 2010.

[18] Y. Todorov, A. M. Andrews, R. Colombelli, S. De Liberato, C. Ciuti, P. Klang, G. Strasser, and C. Sirtori, "Ultrastrong light-matter coupling regime with polariton dots," *Phys. Rev. Lett.*, vol. 105, no. 19, Nov. 2010, Art. no. 196402.

[19] P. Jouy, A. Vasanelli, Y. Todorov, A. Delteil, G. Biasiol, L. Sorba, and C. Sirtori, "Transition from strong to ultrastrong coupling regime in mid-infrared metal-dielectric-metal cavities," *Appl. Phys. Lett.*, vol. 98, no. 23, Jun. 2011, Art. no. 231114.

[20] S. Zanotto, F. P. Mezzapesa, F. Bianco, G. Biasiol, L. Baldacci, M. S. Vitiello, L. Sorba, R. Colombelli, and A. Tredicucci, "Perfect energy-feeding into strongly coupled systems and interferometric control of polariton absorption," *Nature Phys.*, vol. 10, no. 11, pp. 830–834, Oct. 2014.

[21] T. Zhen, J. Zhou, Z. Li, and X. Chen, "Realization of both high absorption of active materials and low ohmic loss in plasmonic cavities," *Adv. Opt. Mater.*, vol. 7, no. 11, Mar. 2019, Art. no. 1801627.

[22] J.-M. Manceau, S. Zanotto, I. Sagnes, G. Beaudoin, and R. Colombelli, "Optical critical coupling into highly confining metal-insulator-metal resonators," *Appl. Phys. Lett.*, vol. 103, no. 9, Aug. 2013, Art. no. 091110.

[23] C. Feuillet-Palma, Y. Todorov, A. Vasanelli, and C. Sirtori, "Strong near field enhancement in THz nano-antenna arrays," *Sci. Rep.*, vol. 3, no. 1, p. 1361, Mar. 2013.

[24] C. Feuillet-Palma, Y. Todorov, R. Steed, A. Vasanelli, G. Biasiol, L. Sorba, and C. Sirtori, "Extremely sub-wavelength THz metal-dielectric wire microcavities," *Opt. Express*, vol. 20, no. 27, pp. 29121–29130, Dec. 2012.

[25] D. Palaferri, Y. Todorov, A. Bigioli, A. Mottaghizadeh, D. Gacemi, A. Calabrese, A. Vasanelli, L. Li, A. G. Davies, E. H. Linfield, F. Kapsalidis, M. Beck, J. Faist, and C. Sirtori, "Room-temperature nine-μm-wavelength photodetectors and GHz-frequency heterodyne receivers," *Nature*, vol. 556, no. 7699, pp. 85–88, Mar. 2018.

[26] Y. Nga Chen, Y. Todorov, B. Askenazi, A. Vasanelli, G. Biasiol, R. Colombelli, and C. Sirtori, "Antenna-coupled microcavities for enhanced infrared photo-detection," *Appl. Phys. Lett.*, vol. 104, no. 3, Jan. 2014, Art. no. 031113.

[27] Y. L. Zheng, P. P. Chen, H. M. Yang, and X. S. Chen, "High-responsivity and polarizatio-discriminating terahertz photodetector coupled by metal-dielectric-metal microcavity," *Appl. Phys. Lett.*, vol. 114, no. 9, Feb. 2019, Art. no. 091105.

[28] Y. Zheng, P. Chen, J. Ding, H. Yang, X. Nie, X. Zhou, X. Chen, and W. Lu, "High intersubband absorption in long-wave quantum well infrared photodetector based on waveguide resonance," *J. Phys. D: Appl. Phys.*, vol. 51, no. 22, May 2018, Art. no. 225105.

[29] J. Lee, M. Tymchenko, C. Argyropoulos, P.-Y. Chen, F. Lu, F. Demmerle, G. Boehm, M.-C. Amann, A. Alú, and M. A. Belkin, "Giant nonlinear response from plasmonic metasurfaces coupled to intersubband transitions," *Nature*, vol. 511, no. 7507, pp. 65–69, Jul. 2014.

[30] R. Gansch, S. Kalchmair, P. Genevet, T. Zederbauer, H. Detz, A. M. Andrews, W. Schrenk, F. Capasso, M. Lončar, and G. Strasser, "Measurement of bound states in the continuum by a detector embedded in a photonic crystal," *Light, Sci. Appl.*, vol. 5, no. 9, Apr. 2016, Art. no. e16147.

[31] F. Mesa, R. Rodriguez-Berral, and F. Medina, "Unlocking complexity using the ECA: The equivalent circuit model as an efficient and physically insightful tool for microwave engineering," *IEEE Microw. Mag.*, vol. 19, no. 4, pp. 44–65, Jun. 2018.

[32] J.-Y. Ding, X.-S. Chen, Q. Li, W.-W. Tang, C.-L. Liu, H.-L. Zhen, Y.-L. Jing, H. Wang, and W. Lu, "The enhanced optical coupling in a quantum well infrared photodetector based on a resonant mode of an air–dielectric–metal waveguide," *Opt. Quantum Electron.*, vol. 47, no. 7, pp. 2347–2357, Jan. 2015.

[33] K. Okamoto, *Fundamentals of Optical Waveguides*. New York, NY, USA: Academic, 2006.

[34] X.-Y. Peng, B. Wang, S. Lai, D. H. Zhang, and J.-H. Teng, "Ultrathin multi-band planar metamaterial absorber based on standing wave resonances," *Opt. Express*, vol. 20, no. 25, pp. 27756–27765, Nov. 2012.

[35] O. Luukkonen, C. Simovski, G. Granet, G. Goussetis, D. Lioubtchenko, A. V. Raisanen, and S. A. Tretyakov, "Simple and accurate analytical model of planar grids and high-impedance surfaces comprising metal strips or patches," *IEEE Trans. Antennas Propag.*, vol. 56, no. 6, pp. 1624–1632, Jun. 2008.

[36] Z. Wang, M. Zhou, X. Lin, H. Liu, H. Wang, F. Yu, S. Lin, E. Li, and H. Chen, "A circuit method to integrate metamaterial and graphene in absorber design," *Opt. Commun.*, vol. 329, pp. 76–80, Oct. 2014.

[37] *Multiphysics Modeling and Simulation Software-COMSOL*. [Online]. Available: https://www.comsol.com
[38] H. A. Haus, *Waves and Fields in Optoelectronics*. Upper Saddle River, NJ, USA: Prentice-Hall, 1984.
[39] D. K. Cheng, *Field and Wave Electromagnetics*. New York, NY, USA: Addison-Wesley, 1989.
[40] R. Zhang, X. G. Guo, J. C. Cao, and H. C. Liu, "Near field and cavity effects on coupling efficiency of one-dimensional metal grating for terahertz quantum well photodetectors," *J. Appl. Phys.*, vol. 109, no. 7, Apr. 2011, Art. no. 073110.
[41] E. Popov, S. Enoch, and N. Bonod, "Absorption of light by extremely shallow metallic gratings: Metamaterial behavior," *Opt. Express*, vol. 17, no. 8, pp. 6770–6781, Apr. 2009.

XUGUANG GUO was born in Liaoning, China. He received the bachelor's and master's degrees in physical electronics from Fudan University, China, in 1997 and 2000, respectively, and the Ph.D. degree in microelectronics and solid-state electronics from the Shanghai Institute of Technical Physics, Chinese Academy of Sciences, in 2003. He is currently a Professor with the University of Shanghai for Science and Technology, China. His major research interest includes terahertz semiconductor optoelectronic devices.

YUXIANG REN was born in Anhui, China. He is currently pursuing the M.S. degree under the supervision of Prof. X. Guo with the University of Shanghai for Science and Technology, Shanghai, China. His current research interest includes graphene modulator.

GUIXUE ZHANG was born in Anhui, China. She is currently pursuing the M.S. degree under the supervision of Prof. X. Guo with the University of Shanghai for Science and Technology, Shanghai, China. Her major research interest includes terahertz quantum well detector.

ANQI YU received the Ph.D. degree in microelectronics and solid-state electronics from the Shanghai Institute of Technical Physics, Chinese Academy of Sciences, Shanghai, China, in 2019. He holds a postdoctoral position with the University of Shanghai for Science and Technology. His current research interests include terahertz detection and modulation based on low-dimensional materials.

XIAOSHUANG CHEN received the Ph.D. degree in condensed matter physics from Nanjing University, Jiangsu, China, in 1995. He was a Research Fellow with the Korea Institute of Advanced Study, The University of Tokyo, Japan, and a Humboldt Research Fellow with Universität Würzburg, Germany. He is currently a Professor with the Shanghai Institute of Technology Physics and the Director of the State Key Laboratory of Infrared Physics. He has coauthored more than 100 publications. His current research interests include infrared photo-electronic material design, high-speed electronic device design, and photonic crystal. He received many national prizes for solving problems in infrared photo-electronics.

YIMING ZHU received the B.S. and M.S. degrees in applied physics from Shanghai Jiao Tong University, Shanghai, China, in 2002 and 2004, respectively, and the Ph.D. degree in electronics engineering from The University of Tokyo, Tokyo, Japan, in 2008. He is currently a Professor with the University of Shanghai for Science and Technology, Shanghai, and the Vice Director with the Shanghai Key Laboratory of Modern Optical System. He has published more than 70 articles on SCI journals. He received the Japanese Government (Monbukagakusho) Scholarship in 2004.